Doxorubicin and siRNA co-delivery System Based on Carbon Dots Inhibits Chemoresistance of Lung Cancer Through MRP1

Luo Hui
Fifth Affiliated Hospital of Sun Yat-sen University
Tang Kexin
SYSU: Sun Yat-Sen University
Lin Xi
SYSU: Sun Yat-Sen University
Huang Yongquan
Fifth Affiliated Hospital of Sun Yat-sen University
Yu Ting
SYSU: Sun Yat-Sen University
Wang Qiang
Chongqing Jiaotong University
Wu Lili
Harbin Normal University
Yang Lei
Harbin Institute of Technology
Hailing Yu (seal101010@163.com)
Sun Yat-Sen University https://orcid.org/0000-0001-8004-6444
Shan Hong
SYSU: Sun Yat-Sen University

Research

Keywords: chemoresistance, co-delivery, siRNA, carbon dots, MRP1

Posted Date: December 29th, 2021

DOI: https://doi.org/10.21203/rs.3.rs-1197591/v1

Abstract

Background

Acquired resistance against chemotherapeutic drugs hinders the clinical efficacy of treatments in lung cancer. To circumvent the developed resistance, we aim to target critical signaling molecules related with chemoresistance through co-delivering siRNA and chemotherapeutics. The co-delivery strategy may address the unmet need to efficiently counteracting the multidrug resistance in treating lung cancer.

Methods

A co-delivery nanosystem that could carry siRNA and DOX simultaneously has been studied in this work. The co-delivery is based on carbon dots was surface-modified with poly-ethylenimine (PEI), and loaded the siMRP1 and chemotherapeutics on the surface with pH-triggered drug release. The CD-PEI was synthesized by one-step microwave assisted method; the PEI were raw materials and passivator during the reaction process that makes CD exhibit excellent optical property.

Results

The CD-PEI was capable of loading and delivering siMRP1 and DOX to tumor and release synchronously in cells by acid-triggered manner.The expression of MRP1 in A549 and A549/ADM cells were successfully knocked down by siRNA. The silencing of MRP1 by co-delivery system could increase DOX accumulation and significantly enhance the inhibitory effect of cell viability. Moreover, the co-delivery system enhances the inhibitory effect of metastatic potential elicited by doxorubicin in A549 and A549/ADM cells.

Conclusion

By suppressing MRP1, the co-delivery system can obviously increase the drug cellular accumulation and inhibit the cell proliferation, migration and invasion of lung cancer, implying its potential application to overcome chemoresistance and enhance therapeutic efficiency in clinical practices.

1. Background

Chemotherapy is an alternative option for advanced patients diagnosed with lung cancer[1]. However, drug resistance inevitably developed during the chemotherapy, leading to high recurrence rate[2, 3]. Effective delivery of anticancer drug to the targeted tissue enhances the drug accumulation in tumor to weaken the side effects. With the advance of nanotechnology, nanomaterials have the advantage to load and selectively release the anti-cancer drugs targeted to the tumor entity, improving treatment efficiency. Cancer cells acquired resistance after drug treatment, leading to less internalization of the chemotherapeutics and reduced the therapeutic effect through plenty of mechanisms, such as overexpression of ATP-binding cassettes which pump the drugs out of cells [4]. Chemoresistance easily developed after several rounds of chemotherapy in treating lung cancer[5]. A plethora of proteins were identified in acquired resistance against chemotherapy drugs in treating lung cancer. The ATP-binding

cassette (ABC) transporters P-glycoprotein and multidrug resistant proteins 1 (MRP1, MRP2, MRP3) were reported to devote to chemoresistance of lung cancer against various agents. Lung resistance related protein (LRP) was also found to play a significant role in developing resistance against lung cancer. However, the mechanisms underlying these molecules are diverse. LRP fulfill its role by redistributing of drugs between cytoplasm and nucleus, while MRP1 was involved in chemoresistance by enhancing efflux of drugs out of cells to weaken toxic effect of drugs. In our previous study, we discovered that CD-PEI-DOX treatment induced remarkable accumulation of doxorubicin in cancer cells, compared with doxorubicin[6]. This prompted us to hypothesize that altered membrane transport of drugs might be involved in CD-PEI-DOX treatment. We tentatively investigated the effect of CD-PEI-DOX on multidrug resistance regulators such as p-glycoprotein and MRP1. We observed that MRP1 changed markedly after CD-PEI-DOX treatment, thus we focused on MRP1 to further delve into the regulation of CD-PEI-DOX on chemoresistance[7, 8]. We aim to analyze how MRP1 was involved in chemoresistance against doxorubicin. Whether MRP1 was involved in uptake of doxorubicin and influencing treatment effect elicited by CD-PEI-DOX remain elusive. Utilizing small interfering RNA (siRNA) to downregulate proteins associated with multidrug resistance, such as MRP1, might represent a promising strategy for reversing drug resistance[9].

The delivery of anti-cancer genes can correct multidrug resistance-related genes and restore the sensitivity of cancer cells to chemotherapy drugs. Co-delivery siRNA targeted relevant resistance gene and chemotherapeutics may overcome the multidrug resistance to chemotherapy[10–13]. Polymer nanoparticles[14], and inorganic nanoparticles have been used as a nanoplatform for co-delivery siRNA and drug[15]. However, several difficulties impede the application co-delivery system. Firstly, the co-delivery requires the synthesis of nanocarrier complex. Secondly, it is hard to accomplish the selective release of co-loaded agents. Carbon dots (CD) is a novel kind of the quantum-sized nanomaterials, which have enormous application potential in bio-imaging, drug carrier, and nanosystems[16–18]. Carbon dots are composed by carbon atoms, exhibiting excellent inherent biocompatibility, have the feasibility in the biotechnology application[19–22]. CD have the capability of delivery chemotherapeutic to the tumor, decrease cytotoxicity, and enhance chemotherapy efficacy[23–25]. And CD with surface-modified groups can carry multiple drugs on the surface simultaneously[26, 27].

In this work, the CD are fabricated by microwave and passivized by polyethyleneimine (PEI). The surface of CD is modified by PEI, as a passivation agent, to enhance the fluorescence intensity of CD and have the capability of loading and delivery siRNA. The siRNA and DOX anti-cancer agents are delivered simultaneously to the targeted tumor by the CD with surface-modified PEI. By suppressing drug efflux pumps, the intercellular uptake of anticancer agents is increased and more drugs located at the perinuclear regions. And the co-delivery system incorporating suppression of MRP1 and anticancer agents could enhance anti-cancer efficacy against chemoresistance in the lung cancer. The real-time tracking of the delivery is realized through the excellent optical property of co-delivery carrier. Our findings would also fasten the clinical potential of co-delivery system with a combination of chemotherapeutics and siRNA sequences.

2. Materials And Methods

2.1 The synthesis of CD-PEI

CD-PEI was fabricated by the microwave-assisted method with PEI-passivated at the surface. The glycerol and PBS solution (pH 7.4) have been mixed, and PEI (MWCO, 25 kDa) was added into the homogeneous solution. The mixed solution has been transformed into a beaker, and placed into a microwave oven for heating 10 minutes. Then, the reaction product was diluted by 10 mL ultrapure water and dialyzed for 2 days to remove the unreacted agents. The solution after dialysis was lyophilized and stored at 4 ℃.

2.2 The characterization of CD-PEI and a nanodrug system based on CD-PEI

The TEM image of CD-PEI was obtained by high-resolution transmission electron microscopy (JEM-2100) and the X-ray photoelectron spectroscopy of CD-PEI and CD-PEI-DOX were measured by a Thermo 250Xi Thermo K-Alpha. The UV-Vis absorbance spectra of the CD-PEI, CD-PEI-DOX, CD-PEI-DOX-siNC, and CD-PEI-DOX-siMRP1 were measured by a Shimadzu UV3600. The PL spectra were characterized by a flourescence spectrofluorometer (Edinburgh, FLS 980-STM). The FTIR spectra were measured by a Thermo Instruments Nicolet 6700.

2.3 The loading and releasing of DOX

The DOX was loaded onto CD-PEI by electrostatic interactions, which has been studied in our previous work[23]. Briefly, the CD-PEI solution mixed with DOX was shaked for 24 h at 4 ℃ and then dialysised for 3 days to remove the excess DOX agent. The 40 nmol/L MRP1 siRNA was added into the CD-PEI-DOX solution and shaked for 24 h at 4 ℃ in order to combine them through electrostatic interactions.

The drug loading efficiency of DOX was calculated by the absobance at 480 nm. The DOX releasing by CD-PEI-DOX-siMRP1 was measured by the drug release experiment as following: 2 mL CD-PEI-DOX-siMRP1 solution was added into a dialysis bag (MWCO, 3 kDa), and soaked into PBS solution. After incubation for different interval, 1 mL PBS solution was gathered and fresh same volume PBS solution was added. The CD-PEI solution was placed under a 5 W UV flashlight with an excitation wavelength of 365 nm. The drug loading efficiency (DLE) was calculated as follows:

DLE% = (amount of DOX in CD-PEI-DOX/amount of DOX) ×100%.

2.4 Cell culture

The human lung cancer cells (A549) and doxorubicin-resistant lung cancer cells (A549/ADM) were cultured in Dulbecco's Modified Eagle's Medium (DMEM). The 10% fetal bovine serum (FBS), 1% penicillin(100 unit mL^{-1}) and streptomycin (100 μg mL^{-1}) (Gibco, Carlsbad, CA, USA) were added into the DMEM solution. The cells were cultured in a incubator with 5% CO_2 at 37 ℃.

2.5 Cell cytotoxicity

The Cell Counting Kit-8 (CCK8) was used to measure the cell viability. 1×10^4 of A549 and A549/ADM cells were seeded in 96-well plates for 24 hours. The PBS, free DOX, CD-PEI-DOX, and CD-PEI-DOX-siMRP1 were added into the DMEM with different concetrations and incubated for 48 hours. Then, the cells were rinsed and added medium with CCK8 for 1 hours. The absorbance at 450 nm was measured by a spectrophotometer.

2.6 In vitro transfection

To evaluate the efficiency of knocking down MRP1 protein, A549 cells ($2x10^5$/well) and A549/ADM cells ($2x10^5$/well) were separately seeded in 6-well plates and incubated for 24h. The solutions of siMRP1-lipid complexes (50 nmol/L siMRP1) or CD-PEI-siMRP1 complexes were prepared before transfection. The two kinds of siMRP1 mixture were separately added to each well. After 12 h transfection, the culture medium was replaced with the fresh complete medium. The cells were incubated for an additional 36 h and the expression of MRP1 protein was detected by flow cytometry.

To evaluate the delivery efficiency of siMRP1, A549 cells ($2x10^5$/well) and A549/ADM cells ($2x10^5$/well) were separately seeded in 6-well plates and incubated for 24h. The siMRP1-lipid complexes (50 nmol/L siMRP1) or CD-PEI-siMRP1 complexes were synthesized by Cy5-labeled siRNA. The two kinds of Cy5-labeled siMRP1 mixture and Cy5-labeled siMRP1 were separately added to each well. After 12 h transfection, the intracellular fluorescence intensity was detected via laser scanning confocal microscope and flow cytometry (FCM).

2.7 Intracellular drug release

A549 and A549/ADM cells were seeded and cultured on the Φ15 mm glass battern cell culture dish, respectively. The PBS, free DOX (20μg/mL), CD-PEI-DOX (DOX concetration, 20μg/mL), CD-PEI-DOX-siNC (DOX concetration, 20μg/mL), and CD-PEI-DOX-siMRP1 (DOX concetration, 20μg/mL) have been added into the culture dish and incubated for 24 hours. After incubation, the cells were rinsed by PBS and observed by laser scanning confocal microscopy (Zeiss LSM 880, Jena, Germany). The cell nucleus is dyed by RedDot^{TM} 1. A549/ADM cells manmospheres were seeded in the confocal dish and incubated with nanodrug for 24 hours.

2.8 Cellular uptake *in vitro*

6×10^5 of A549 and A549/ADM cells have been seeded in the petri dish, respectively. And the cells were treated by different groups, such as PBS, free DOX, CD-PEI-DOX, CD-PEI-DOX-siNC, and CD-PEI-DOX-siMRP1 for different inbucation time. And the cells were collected to measure the geometric mean fluorescence intensity by flow cytometry in Y610-mCHERRY channel (Beckman cytoflex LX).

2.9 The transwell assays

The migration and invasion assays of the A549/ADM cells and A549 cells evaluating metastasis potential were performed in 24-well transwell chambers with 8 μm size pores (Costar, Washington, D.C., USA). And the pores were covered with 100 μL of Matrigel (BD, USA) in the invasion assay. A549/ADM and A549 were added PBS, DOX, CD-PEI-DOX, CD-PEI-DOX-siNC and CD-PEI-DOX-siMRP1 and incubated for 24 hours. The DOX concetrations of A549/ADM and A549 are 60 μg/mL and 30 μg/mL, respectively. Then, 8×10^4 cells in 200 μL serum-free DMEM were seeded in the upper chambers and 700 μL of medium supplemented with 10% fetal bovine serum was added in the lower chamber. After 24h of incubation in 37°C, 5% CO_2, the upper chambers were removed, and cells on the lower face of the membranes were fixed with 4% fixative solution (Solarbio, Beijing, China) and stained with Crystal violet. We counted the number of migrated or invaded cells under 5 randomly selected fields at ×10 magnification by inverted light microscope (Leica DMi1, Wetzlar, Germany) for three times independently.

2.10 RNA isolation and qPCR analysis

Total Cell RNA isolation and cDNA synthesis were finished with the PrimeScript™ RT reagent Kit (TaKara Bio, USA) following the protocol. The concentration and integrity of RNA was determined using the 260/280 ratios generated by a Nano-drop UV spectrophotometer. Gene-specific primers were designed and synthesized by IGE BIOTECHNOLOGY (Guangzhou, China). qPCR was performed using PrimeScript RT Enzyme Mix I according to the manufacturer's instructions in CFX96™ Real-Time System (C1000 Thermal Cycler Class, Bio-Rad, California, USA). The two-step PCR conditions used are as follows: Pre-denaturation at 95°C for 30 second; 40 cycles of (denaturation at 95°C for 5 second, annealing and extension at 60°C for 30 second), and denaturation for 10 second. And then melting curve stage was followed from 60 to 95°C with increment 0.5°C for 20 second while scanning for fluorescence. Relative quantitation was performed using the $2-\Delta\Delta Ct$ method and data were normalized against GAPDH. Primers sequences for MRP1 and GAPDH are as follows: MRP1: 5'-CCGTGTACTCCAACGCTGACAT-3' and 5'-ATGCTGTGCGTGACCAAGATCC-3'; GAPDH: 5'-TGTGGGCATCAATGGATTTGG-3' and 5'-ACACCATGTATTCCGGGTCAAT-3'.

2.11 In vitro transfection

A549/ADM cells (4×10^5) were seeded in 6-well plates and incubated for 24h. The solutions of siMRP1-lipid complex complexes (50 nmol/L siMRP1) or CD-PEI-siMRP1 complexes were prepared before transfection. The medium was replaced by 1 mL Opti-MEM per well and the two kinds of siMRP1 mixture were separately added to each well. After 12 h transfection, the culture medium was replaced with the fresh complete medium and cells were incubated for an additional 36 h for flow cytometry. The siRNA are purchased from RiboBio Co., Ltd.(Guangzhou, China) and the number of NC (Negative control) is siN0000001-1-5 siR. The sequences for siMRP1 are as follows: stB0001371B genOFFTM st-h-MRP1_001: GACCTCCGCTTCAAGATCA; stB0001371B genOFFTM st-h-MRP1_002: CCGTCTACGTGACCATTGA; stB0001371B genOFFTM st-h-MRP1_003: CTGGGCTTATTTCGGATCA.

2.12 Western blot assays

Western blot assays were carried out as previously described[28]. Briefly, total cell lysates were prepared in RIPA buffer (Beyotime, Shanghai, China). and proteins were separated by the sodium dodecyl sulfate-polyacrylamide gel electrophoresis (SDS-PAGE) and transferred to nitrocellulose membranes. After blocking with 5% skim milk for 2 h, the membranes were incubated with the primary antibodies against MRP1 (Cell Signaling Technology, Boston, MA, USA), P-gp (GeneTex, Irvine, CA, USA), and then incubated with the secondary HRP-conjugated antibody (1:5000, Zhongshan Goldenbridge, Beijing, China). Protein bands were visualized using ECL detection reagent and normalized by β-actin (Cell Signaling Technology, Cell Signaling Technology, Boston, MA, USA). Triplicate individual experiments were performed in this study.

2.13 Sphere forming assays.

A549 and A549/ADM cells were treated by PBS, free DOX, CD-PEI-DOX, CD-PEI-DOX-siNC, CD-PEI-DOX-siMRP1 for 24h, respectively. The cells were digested and seeded onto 6-well plates and cultured in sphere forming medium: DMEM/F12 medium (GIBCO) contained with 4 μg/mL insulin, B27 (1:50), 20 ng/mL EGF and 10 ng/mL FGF. The morphology and diameters of spheres were measured after an additional 5 days.

2.14 Animal Study in vivo

All animal studies were approved by Animal ethics committee of the Fifth Affiliated Hospital Sun Yat-sen University. Briefly, A549/ADM cells were subcutaneously inoculated into 4 weeks old male Balb/c nude mice to construct xenograft models. When tumors grew to palpable size, DOX and CD-PEI-DOX-siMRP1 were injected through tail vein. The bio-distribution of drugs were visualized by in vivo image system (IVIS) equipment. Hemolysis experiment were performed to assess the biocompatibility of drugs. The targeting of drugs on tumor were viusualized and photographed as the indicated time points.

2.15 Immunohistochemical assays

Tumor and organs were obtained after mouse were scarificed humanely. Slices were prepared from frozen tissues. Immunohistochemical staining were conducted as previously described[23]. Hematoxylin and eosin (H&E) staining (ZSBG-BIO, Beijing, China) were carried out to investigate the toxic effect of drugs. Representative pictures were shown and the distribution of different drugs were visulized undrer optical microscopes (BX53 System Microscope, Olympus, Japan).

2.16 Statistical analysis

The data between groups was statistical analyzed by Student's t-test. $p<0.05$ was used as the criterion for statistical significance.

3. Results And Discussion

3.1 The characteristic of CD-PEI and nanodrug system based on CD-PEI

The TEM images showed that CD-PEI was uniform and spherical, with an average size of 4.25 nm which obtained by measuring the sizes of hundreds CD nanoparticles in TEM images. It is indicated that the average diameter of CD-PEI is 5.503 nm measured by dynamic light scattering (DLS), which is because of the hydration layer. CD-PEI was dark yellow under white light and well-distributed in aqueous solution. Under the UV light, the CD-PEI solution had obvious green emission indicating that CD-PEI had excellent fluorescence property, as shown in Fig. S1. The photoluminescence (PL) spectrum of CD-PEI and CD-PEI-DOX-siMRP1 had been characterized by various excitation wavelengths with 20 nm increments. The emissions of CD-PEI are red-shifted with the increase of the excitation wavelength. The CD-PEI exhibited excellent and stable PL property that is beneficial for the tracking of drug delivery *in vivo*. The emission in carbon dots could result from the nanometer quantum confinement effect[29, 30]. In addition, the CD-PEI also possess excitation-dependent emission behavior[31, 32], that when the excitation wavelength increase from 330 nm to 510 nm, the emission peak shift from 450 to 600 nm. The multicolor PL behavior may result from the uneven distribution of emission traps on the surface of carbons dots[33]. When the excitation wavelength is 350 nm, the emission intensity is highest. In this work, we studied the PL behavior of CD-PEI-DOX-siMRP1 through increasing excitation wavelength from 270 to 510 nm. Due to the loading of DOX agents, the optical property of CD-PEI has changed. The PL spectra of CD-PEI and CD-PEI-DOX-siMRP1 were obviously different due to the addition of DOX. The CD-PEI-DOX-siMRP1 had no obvious emission peak when the excitation wavelength is lower than 330 nm. When excitation wavelengths increase from 350 nm to 510 nm, the emission intensity of CD-PEI-DOX-siMRP1 is increasing, and reaches maximum at 470 nm. The change of emission peak confirmed the DOX has been successfully loaded on the surface of CD-PEI[34].

There is obvious absorption band correspond to the O-H stretching in the FTIR spectrum of the CD and PEI, as shown in Fig. 2F and Fig. 2S. The absorption peaks centered at 1096 cm^{-1} and 1655 cm^{-1} are corresponded to the C-O and C=O stretching, respectively. The absorption bands at 1453 cm^{-1} and 2949 cm^{-1} are corresponded to the C-H and CH_2 stretching, respectively. The UV-Vis spectrum of CD-PEI in Fig. 2G had two bands at 304 nm and 346 nm, corresponding to the π-π^* transition and n-π^* transition[35–37]. The CD-PEI-DOX, CD-PEI-DOX-siNC, and CD-PEI-DOX-siMRP1 had a broad peak band at 480-600 nm among which was the DOX characteristic absorbance peak. These results confirmed that DOX was loaded on the surface of CD-PEI, and the drug loading efficiency of CD-PEI was 16.7%.

The drug release behavior of CD-PEI-DOX-siMRP1 was revealed by *in vitro* release test. The free DOX release totally during 50 hours, while CD-PEI-DOX-siMRP1 prolongs the drug release time up to 72 hours when pH was 5.2. CD-PEI-DOX-siMRP1 released fairly minimal DOX under pH 7.4 and illustrated that the nanocarrier would avoid the toxic effect of excessive DOX accumulation in normal tissue and cell. When the pH changed from 7.4 to 5.2, the release amount of DOX from CD-PEI-DOX-siMRP1 increased about 5-times indicating that CD-PEI-DOX-siMRP1 was pH-sensitive and triggered the release of DOX by acid environment. The advantage of selective drug release behavior of nanosystem could enhance the therapeutic effect of tumor and decrease the toxic to normal tissue.

The information of the chemical composition and functional groups of nanodrug were characterized by X-ray photoelectron spectroscopy (XPS) in Fig. 2I. As shown in Fig. 2, the XPS spectra of CD-PEI-DOX-siMRP1 exhibits three peaks corresponding to C1s peak at 284.5 eV, N1s peak at 399.5 eV, and O1s peak at 531.5 eV, respectively. This result indicates that CD-PEI-DOX-siMRP1 are mainly composed of C, N, and O, with some small inorganic elements due to the synthesis while attaining a solution system at pH 7.4 with PBS[38]. The C1s spectrum of CD-PEI-DOX-siMRP1 (Fig. 2J) shows four peaks at 284.8 eV, 285.8 eV, 287.7 eV, and 288.3 eV, which are attributed to C-C/C=C (78.4%), C-N/C-OH (16.4%), C=O (2.7%), and O-C=O (2.5%), respectively. The N1s spectrum of CD-PEI-DOX-siMRP1 (Fig. 2K) exhibits two components located at 398.9 eV and 400.2 eV, assigned to C=C-N (80.5%) and N-$(C)_3$ (19.5%) groups. The O1s spectrum of CD-PEI-DOX-siMRP1 (Fig. 2L) shows two peaks at 531.0 eV and 531.9 eV, which are corresponded to the C=O (47.7%) and C-OH/C-O-C (52.3%) groups. As shown in Table S1, the change in the chemical groups and the percentage of the nanodrug in the spectra gives further evidence of successful complex conjugation.

3.2 MRP1 was involved in chemoresistance of A549 against CD-PEI-DOX.

Failure of the chemotherapy to malignant tumor was mainly attributable to insensitivity to drugs. Elucidating the mechanisms how tumor cells modulate the chemoresistance was critical for improving the chemotherapeutic effect of various anticancer drugs. We previously confirmed that CD-PEI-DOX treatment in hepatocellular carcinoma inhibit tumor growth through actively targeting tumors[23]. This led us to postulate: whether CD-PEI-DOX would elicit side effects on malignant tumors such as increasing chemoresistance in lung cancer. We firstly tentatively detected the expression of molecules associated with chemoresistance including p-glycoprotein (P-gp), and MRP1 in adherent, sphere and chemoresistant lung cancer cell line A549. From Fig. 3A, we vividly observed that molecules related with chemoresistance were elevated in spheres formed by A549 cells, which were considered to bear more traits of stemness compared with adherent cells. Consistently, the expression of these molecules elevated most in A549/ADM cells. These results show that A549/ADM cells expressed a panel of molecules involved in chemoresistance. Subsequently, we analyzed the cell viability of A549 and chemoresistant A549/ADM cells after doxorubicin treatment (Fig. 3B). We discovered that A549/ADM cells were resistant to doxorubicin treatment. The involvement of MRP1 in chemoresistance of A549 cells against doxorubicin was investigated by tentatively knocking down the expression of MRP1 using siRNA transfection. We determined the best knockdown efficiency of siRNA targeting MRP1 using qPCR methods and western blot. From Fig. 3C-E, we determined siRNA #2 was the most efficient sequence targeting MRP1 in both A549 and A549/ADM cells.

The transfection efficiency of siMRP1 was detected by laser scanning confocal microscope. The siMRP1 was transfected into A549 and A549/ADM cells using lipo or CD-PEI vectors. As shown in Fig. 4A, CD-PEI delivered the sequences targeting MRP1 to cells most efficiently compared with lipo and sequences alone. The flow cytometry results are consistent with the confocal images (Fig. 4B). The results confirmed that CD-PEI is an ideal carrier for mediating siMRP1 transfection in lung cancer cells.

To clarify the influence of the serum on the delivery effect of cationic vectors, we incubate different vectors with siRNA as indicated with increasing concentration of serum. As shown in Fig. 5A-B, CD-PEI delivers siRNA most efficiently in present of different concentration of serum. In addition, the knocking down effect of siMRP1 was evaluated by flow cytometry in Fig. 5C-F. The expression of MRP1 in A549 and A549/ADM cells were decreased by the transfection of siMRP1 mediated by CD-PEI. The results collectively revealed siRNA sequences were successfully delivered to A549 and A549/ADM cells by CD-PEI with strong stability. Importantly, the expression of MRP1 in A549 and A549/ADM using CD-PEI as transfection vector is much lower than lipo indicating the enhanced transfection efficiency and suppression of MRP1 expression induced by CD-PEI delivery.

Based on above findings, we explore how MRP1 suppression influences the viability and chemoresistance of lung cancer cells? CD-PEI-DOX was conjugated with siMRP1 and CCK8 assays were performed to analyze the cell viability after treatment by various drugs. The IC_{50} of drugs in both A549 and A549/ADM cells were calculated from three independent cell toxicity experiments. As shown in Fig. 5G-5H and Table 1, the IC_{50} of free doxorubicin in A549/ADM cells was approximately 5 fold higher compared with A549 cells. Accordingly, the IC_{50} of CD-PEI-DOX in A549/ADM cells were markedly higher (18.19μg/mL) than that (6.72μg/mL) in the A549 cells. When CD-PEI-DOX were loaded with MRP1 siRNA sequences, the cells became more vulnerable to CD-PEI-DOX, IC_{50} was only 17.4μg/mL in A549/ADM cells. The CD-PEI has been proved to be non-toxic to cancer cells and normal cells, as shown in Fig. S3. Based on these findings, we conclude that the free DOX exhibited different toxic effects to A549 and A549/ADM cells. CD-PEI-DOX-siMRP1 inhibited viability of A549/ADM cells more markedly compared with free DOX and CD-PEI-DOX groups at all-time points. It implied that CD-PEI-DOX-siMRP1 might possess better antitumor effect than DOX and CD-PEI-DOX. CD-PEI-DOX-siMRP1 possesses high toxicity to A549/ADM due to the co-delivery and synergistic effect of siRNA and DOX, indicating that the MRP1 was critically involved in chemoresistance of A549/ADM cells against doxorubicin. The CD-PEI has the capability of transfecting siRNA to the cells and interfere the expression of MRP1. To further support the conclusion, Ki67, a proliferation marker was immunostained and observed under confocal microscopes. The results show that CD-PEI-DOX-siMRP1 inhibited the proliferation of A549 and A549/ADM cells as indicated in Figure 5I-J.

Table 1

IC_{50} of Free DOX, CD-PEI-DOX, CD-PEI-DOX-siMRP1 in A549 and A549/ADM cells

IC50(μg/mL)		
A549	Free DOX	26.993
	CD-PEI-DOX	6.72
	CD-PEI-DOX-siMRP1	5.692
A549/ADM	Free DOX	130.626
	CD-PEI-DOX	18.19
	CD-PEI-DOX-siMRP1	17.4

These results led us to postulate: whether MRP1 was induced by CD-PEI-DOX and suppressing MRP1 would reverse this effect? To test our hypothesis, we treated both A549 and A549/ADM cells with the indicated drugs and analyzed the expression of MRP1 after treatment using western blot and flow cytometry. As demonstrated in Fig. 6A-B, the expression of MRP1 increased markedly in case of free DOX treatment. In contrast, MRP1 expression in both A549 and A549/ADM cells decreased after siRNA targeting MRP1 was loaded on CD-PEI-DOX particles.

3.3 The internalization of DOX and nanodrug system based on CD-PEI

The cellular uptake of free DOX, and CD-PEI-DOX-siMRP1 has been studied by laser scanning confocal microscopy in Fig. 7A. The A549 and A549/ADM cells were incubated for 24 hours with PBS, free DOX, CD-PEI-DOX, CD-PEI-DOX-siNC, and CD-PEI-DOX-siMRP1, respectively. The results revealed that more CD-PEI-DOX-siMRP1 is uptake by the cancer cells and located in the perinuclear regions and the nuclei. The phenomenon revealed that the CD-PEI-DOX-siMRP1 could enhance the permeability of DOX into the nuclei, which is beneficial to increase the therapeutic efficiency of DOX. In the A549/ADM, CD-PEI-DOX-siMRP1 may obviously increase the uptake efficiency of the DOX into the cell, and enter the A549/ADM more than the free DOX group, for the reason that the co-delivery system may increase the internalization of DOX into the cells.

The internalization of DOX has further been measured by flow cytometry. Fig. 8 depicts the uptake in A549 and A549/ADM cells during the different intervals. The group incubated with CD-PEI-DOX-siMRP1 have higher mean fluorescence intensity than other group in both A549 and A549/ADM, indicated that CD-PEI-DOX-siMRP1 could delivery more DOX into cell. The cellular uptake of free DOX is lower than other treated groups at every interval in both A549 and A549/ADM cells. The nanodrug could decrease the drug efflux and gather high intracellular concentration of the drug, because the nanodrugs may bypass the efflux pumps. And in the A549/ADM cells, the uptake amount of CD-PEI-DOX-siMRP1 is higher than other groups, results from the disrupting of siRNA to cellular pathway. This result indicated that the disturbing

MRP1 could enhance the uptake of nanodrug effectively. The co-delivery DOX and siRNA would more effective in overcoming resistance of cancer cells.

The permeability of CD-PEI-DOX-siMRP1 into the cancer cell spheres has been investigated using the Z-stack mode of laser scanning confocal microscopy. The Z-stack mode could be used to observe the penetrate situation of different treatment by gaining the different layers of the cell mammosphere. The results revealed that the group treated by free DOX has the weakest permeability among all the groups. And the CD-PEI-DOX-siMRP1 could penetrate the inner region of mammosphere, as shown in Fig. 9. This result confirmed that the CD-PEI-DOX-siMRP1 could have the permeability to enter into the inner entity of tumor tissue, which can maximize the therapeutic effect.

3.4 CD-PEI-DOX-siMRP1 enhanced the inhibitory effect on stemness and metastatic potential elicited by doxorubicin

Stemness and metastasis were reported to be associated with recurrence and poor prognosis of patients. We broaden our study to explore the effect of our co-delivery system on metastasis and stemness of lung cancer cells. Research into the regulatory effect of CD-PEI-DOX-siMRP1 would help to explain its possible clinical application with regards to suppressing tumorigenesis and recurrence. To address this, we used the Transwell assay to study the migration and invasion in A549 and A549/ADM cells affected by respective drugs. Both A549 and A549/ADM treated with DOX, CD-PEI-DOX and CD-PEI-DOX-siNC and CD-PEI-DOX-siMRP1 decreased migration and invasion compared to the control, with migration counts shown in Fig. 10, respectively. The results indicated that CD-PEI-DOX and CD-PEI-DOX-siNC and CD-PEI-DOX-siMRP1 generated stronger inhibitory effects than free DOX. We found that nanodrug based on CD-PEI distinctly inhibited the migration and invasion of both A549/ADM and ADM cells compared with the group treated by free DOX. After silencing MRP1, the migration and invasion were more obviously inhibited by CD-PEI-DOX treatment in A549/ADM cells. These results collectively showed that MRP1 is critical for mediating the prometastatic effect of A549 against doxorubicin.

Stemness is widely implicated in chemoresistance of cancer against drugs. To clarify to regulate stemness in lung cancer by MRP1, we conducted sphere-forming assays. As revealed in Fig. 11, CD-PEI-DOX-siMRP1 decreased the sphere-forming ability in A549 cells, which are same in A549/ADM treated by CD-PEI-DOX-siMRP1. It implied that MRP1 was critically involved in migration and invasion of A549/ADM cells. Combined with results, a conclusion could be drawn from findings that suppressing MRP1 expression attenuated the resistance to regulation of stemness, migration and invasion induced by CD-PEI-DOX in DOX-resistant A549 cells.

3.5 Targeting and biocompatibility analysis of CD-PEI-DOX-siMRP1

Based on the *ex vivo* results, we conducted *in vivo* experiments to analyze the targeting of CD-PEI-DOX-siMRP1. As shown in Fig. 12A, specific signal of CD-PEI-DOX-siMRP1 particles were observed, while no marked signal was seen in free doxorubucin treated group. CD-PEI-DOX-siMRP1 located on tumors specfically at 12h. Tumors and organs were harvested, the fluorescence intensity was stastistically analyzed (n=3). CD-PEI-DOX-siMRP1 exhibited strong signal on tumors compared with DOX group (Fig.

12B-C). Hemolysis assays were conducted to analyze the toxic effect of our nanodrugs. The results revealed that CD-PEI-DOX-siMRP1 have no obvious toxic effect on blood among all groups, even at high concentration. Triton X-100 was included as a positive control (Fig. 12D-E). Strong biocompatibility of CD-PEI-DOX-siMRP1 could be concluded since no obvious changes were seen in routine blood test (Fig. 12F). Subsequently, slices from organs of each group were obtanied and subjected to H&E staining. No destructive structures of drugs on different organs were seen (Fig. 12G). These results collectively show that CD-PEI-DOX-siMRP1 consistently target tumor and bear good biocompatibility and no obvious toxic effect *in vivo*.

4. Conclusion

In this work, we offered a new approach to overcome the chemoresistance through a strategy of combining siRNA targeted to MRP1 with chemotherapeutic by the co-delivery system based on CD-PEI. The surface of carbon dots was decorated with PEI groups, being able to carrying siRNA, and the DOX agent was loaded through electrostatic interactions. The co-delivery systems effectively loaded and released siRNA and DOX agents to the targeted tumor, overcoming the resistance to chemotherapy. By suppressing MRP1, CD-PEI-DOX-siMRP1 can obviously increase the drug intercellular accumulation and inhibit the proliferation of cancer cells. Additionally, the migration and invasion of A549/ADM cells were inhibited by CD-PEI-DOX-siMRP1. These results confirmed the co-delivery systems improve the therapeutic efficiency and overcome the chemoresistance. CD-PEI-DOX-siMRP1 co-delivery systems could inhibit the proliferation, migration, and invasion of the cancer cell because of the synergistic treatment from siRNA and anti-cancer agent. These works have laid the foundation for exploring the application of anti-cancer drug chemotherapy-resistant delivery systems in the treatment of lung cancer.

Abbreviations

CD:

carbon dots

PEI:

poly-ethylenimine

DOX:

doxorubicin

siRNA:

small interfer RNA

ATP:

Adenosine triphosphate

IC50 :

half maximal inhibitory concentration

MRP1:

multidrug resistance-associated protein 1

A549：

human non-small cell lung carcinoma cell line

A549/ADM:

multidrug resistant human non-small cell lung carcinoma cell line

QDs:

quantum dots

PL:

photoluminescence

CCK8:

the Cell Counting Kit-8

SDS-PAGE:

sodium dodecyl sulfate-polyacrylamide gel electrophoresis

PVDF:

polyvinylidene difluoride

IVIS:

in vivo image system

DLS:

dynamic light scattering

ABCG2:

ATP-binding cassette transporter, sub-family G, member 2

P-gp:

P-glycoprotein

Declarations

Ethics approval and consent to participate

The study received approval from the institutional review board of the Fifth Affiliated Hospital Sun Yat-sen University.

Consent for publication

Not applicable.

Declaration of interest

The authors declare that they have no known competing financial interests or personal relationships that could have appeared to influence the work reported in this paper.

Availability of data and materials

Data sharing is not applicable to this article as no datasets were generated or analyzed during the current study.

Funding:

The Fundamental Research Funds for the Central Universities (19ykpy42)

The Guangdong Basic and Applied Basic Research Foundation (2020A1515011001)

Author contributions:

Yu Hailing performed the experiments including synthesis and characterization of the nanodrug and wrote the whole paper. Luo Hui carried out the in vivo experiments with Lin Xi. Huang Yin conducted in vitro experiments together with Tang Kexin. All the co-first author analyzed all the data in the article. Yang Lei, and Wu Lili helped to conduct the synthesis and characterization of the drug. Yu Ting helped to perform in vitro experiments. Shan Hong designed all the experiments.

Acknowledgments

We owe gratitude to Huang Yongquan for his support in hemolysis and routine blood test experiments. We also appreciate guidance from Zhang Qianqian in trans-well experiments. This work was supported by the Guangdong Basic and Applied Basic Research Foundation (2020A1515011001).

References

1. F. Bray, A. Jemal, N. Grey, J. Ferlay and D. Forman, "Global cancer transitions according to the Human Development Index (2008-2030): a population-based study," *Lancet Oncol* vol. 13, no. 8, pp. 790-801, 2012.

2. R. J. Kathawala, P. Gupta, C. R. Ashby and Z.-S. Chen, "The modulation of ABC transporter-mediated multidrug resistance in cancer: A review of the past decade," *Drug Resistance Updates*, vol. 18, pp. 1-17, 2015.

3. M. Bar-Zeev, Y. D. Livney and Y. G. Assaraf, "Targeted nanomedicine for cancer therapeutics: Towards precision medicine overcoming drug resistance," *Drug Resistance Updates*, pp. 15-30, 2017.

4. M. M. Gottesman, "Mechanisms of Cancer Drug Resistance," *Annual Review of Medicine*, vol. 53, no. 1, pp. 615-627, 2002.

5. D. C. Ihde, "Chemotherapy of lung cancer," *N Engl J Med*, vol. 327, no. 20, pp. 1434-1441, 1992.

6. Y. Hailing, L. Xiufang, W. Lili, L. Baoqiang, H. Kaichen, H. Yongquan, Z. Qianqian, M. Chaoming, R. Xiaoshuai, Z. Rui, L. Hui, P. Pengfei and S. Hong, "Doxorubicin-loaded fluorescent carbon dots with PEI passivation as a drug delivery system for cancer therapy," *Nanoscale*, vol. 12, no. 33, pp. 17222-17237, 2020.

7. J. F. Lu, D. Pokharel and M. Bebawy, "MRP1 and its role in anticancer drug resistance," *Drug Metab Rev*, vol. 47, no. 4, pp. 406-419, 2015.

8. R. W. Robey, K. M. Pluchino, M. D. Hall, A. T. Fojo, S. E. Bates and M. M. Gottesman, "Revisiting the role of ABC transporters in multidrug-resistant cancer," *Nature Reviews Cancer*, vol. 18, no. 7, pp. 452-464, 2018.

9. T. Du, J. G. Liang, N. Dong, L. Liu, L. R. Fang, S. B. Xiao and H. Y. Han, "Carbon dots as inhibitors of virus by activation of type I interferon response," *Carbon*, vol. 110, pp. 278-285, 2016.

10. O. Taratula, "Innovative Strategy for Treatment of Lung Cancer: Inhalatory Codelivery of Anticancer Drugs and siRNA for Suppression of Cellular Resistance," *Journal of Drug Targeting*, vol. 19, no. 10, pp. 900-914, 2011.

11. C. Yang, K. K. Chan, W.-J. Lin, A. M. Soehartono, G. Lin, H. Toh, H. S. Yoon, C.-K. Chen and K.-T. Yong, "Biodegradable nanocarriers for small interfering ribonucleic acid (siRNA) co-delivery strategy increase the chemosensitivity of pancreatic cancer cells to gemcitabine," *Nano Research*, vol. 10, no. 9, pp. 3049-3067, 2017.

12. C. Yang, R. Hu, T. Anderson, Y. Wang, G. Lin, W.-C. Law, W.-J. Lin, Q. T. Nguyen, H. T. Toh, H. S. Yoon, C.-K. Chen and K.-T. Yong, "Biodegradable nanoparticle-mediated K-ras down regulation for pancreatic

cancer gene therapy," *Journal of Materials Chemistry B*, vol. 3, no. 10, pp. 2163-2172, 2015.

13. K. H. Moss, P. Popova, S. R. Hadrup, K. Astakhova and M. Taskova, "Lipid Nanoparticles for Delivery of Therapeutic RNA Oligonucleotides," *Molecular Pharmaceutics*, vol. 16, no. 6, pp. 2265-2277, 2019.

14. S. Chen, J. Deng and L.-M. Zhang, "Cationic nanoparticles self-assembled from amphiphilic chitosan derivatives containing poly(amidoamine) dendrons and deoxycholic acid as a vector for co-delivery of doxorubicin and gene," *Carbohydrate Polymers*, vol. 258, pp. 117706, 2021.

15. M. Creixell and N. A. Peppas, "Co-delivery of siRNA and therapeutic agents using nanocarriers to overcome cancer resistance," *Nano Today*, vol. 7, no. 4, pp. 367-379, 2012.

16. N. Licciardello, S. Hunoldt, R. Bermann, G. Singh, C. Mamat, A. Faramus, J. L. Z. Ddungu, S. Silvestrini, M. Maggini and L. De Cola, "Biodistribution studies of ultrasmall silicon nanoparticles and carbon dots in experimental rats and tumor mice," *Nanoscale*, pp. 10.1039.C1038NR01063C, 2018.

17. S. Hettiarac, R. Graham, K. J. Mintz, Y. Zhou, S. Vanni, Z. Peng and R. Leblanc, "Triple conjugated carbon dots as a nano-drug delivery model for glioblastoma brain tumors," *Nanoscale*, 2019.

18. N. Gao, W. Yang, H. Nie, Y. Gong, J. Jing, L. Gao and X. Zhang, "Turn-on theranostic fluorescent nanoprobe by electrostatic self-assembly of carbon dots with doxorubicin for targeted cancer cell imaging, in vivo hyaluronidase analysis, and targeted drug delivery," *Biosens Bioelectron*, vol. 96, pp. 300-307, 2017.

19. K. J. Chen, Y. L. Chiu, Y. M. Chen, Y. C. Ho and H. W. Sung, "Intracellularly monitoring/imaging the release of doxorubicin from pH-responsive nanoparticles using Förster resonance energy transfer," *Biomaterials*, vol. 32, no. 10, pp. 2586-2592, 2011.

20. S. D. Hettiarachchi, E. C. Kirbas, H. Makhlouf, E. S. Seven and R. M. Leblanc, "pH and redox triggered doxorubicin release from covalently linked carbon dots conjugates," *Nanoscale*, vol. 13, no. 10, 2021.

21. H. Luo, K. Tang, K. Huang, X. Lin and H. Yu, "Doxorubicin and siRNA Co-Delivery System Based on Carbon Dots Inhibits Chemoresistance of Lung Cancer," 2021.

22. J. Zhu, H. Chu, J. Shen, C. Wang and Y. Wei, "Green preparation of carbon dots from plum as a ratiometric fluorescent probe for detection of doxorubicin," *Optical Materials*, vol. 114, pp. 110941, 2021.

23. H. Yu, X. Lv, L. Wu, B. Li and H. Shan, "Doxorubicin-loaded fluorescent carbon dots with PEI passivation as a drug delivery system for cancer therapy," *Nanoscale*, vol. 12, no. 33, pp. 17135-17558, 2020.

24. S. Karimi and H. Namazi, "Simple preparation of maltose-functionalized dendrimer/graphene quantum dots as a pH-sensitive biocompatible carrier for targeted delivery of doxorubicin," *International Journal of Biological Macromolecules*, vol. 156, no. 9, 2020.

25. P. Wolski, "Molecular Dynamics Simulations of the pH-Dependent Adsorption of Doxorubicin on Carbon Quantum Dots," *Molecular Pharmaceutics*, vol. 18, no. 1, 2020.

26. H. Ding, F. Y. Du, P. C. Liu, Z. J. Chen and J. C. Shen, "DNA-Carbon Dots Function as Fluorescent Vehicles for Drug Delivery," *Acs Applied Materials & Interfaces*, vol. 7, no. 12, pp. 6889-6897, 2015.

27. S. Karthik, B. Saha, S. K. Ghosh and N. D. P. Singh, "Photoresponsive quinoline tethered fluorescent carbon dots for regulated anticancer drug delivery," *Chemical Communications*, vol. 49, no. 89, pp. 10471-10473, 2013.

28. X. Lv, H. Yu, Q. Zhang, Q. Huang, X. Hong, T. Yu, H. Lan, C. Mei, W. Zhang and H. Luo, "SRXN1 stimulates hepatocellular carcinoma tumorigenesis and metastasis through modulating ROS/p65/BTG2 signalling," *Journal of Cellular and Molecular Medicine*, vol. 24, pp. 10714-10729, 2020.

29. Y. P. Sun, B. Zhou, Y. Lin, W. Wang, K. A. S. Fernando, P. Pathak, M. J. Meziani, B. A. Harruff, X. Wang, H. F. Wang, P. J. G. Luo, H. Yang, M. E. Kose, B. L. Chen, L. M. Veca and S. Y. Xie, "Quantum-sized carbon dots for bright and colorful photoluminescence," *Journal of the American Chemical Society*, vol. 128, no. 24, pp. 7756-7757, 2006.

30. S. N. Baker and G. A. Baker, "Luminescent Carbon Nanodots: Emergent Nanolights," *Angewandte Chemie-International Edition*, vol. 49, no. 38, pp. 6726-6744, 2010.

31. J. Hou, J. Yan, Q. Zhao, Y. Li, H. Ding and L. Ding, "A novel one-pot route for large-scale preparation of highly photoluminescent carbon quantum dots powders," *Nanoscale*, vol. 5, no. 20, pp. 9558-9561, 2013.

32. S. W. Zhang, J. X. Li, M. Y. Zeng, J. Z. Xu, X. K. Wang and W. P. Hu, "Polymer nanodots of graphitic carbon nitride as effective fluorescent probes for the detection of Fe3+ and Cu2+ ions," *Nanoscale*, vol. 6, no. 8, pp. 4157-4162, 2014.

33. Y.-P. Sun, B. Zhou, Y. Lin, W. Wang, K. A. S. Fernando, P. Pathak, M. J. Meziani, B. A. Harruff, X. Wang, H. Wang, P. G. Luo, H. Yang, M. E. Kose, B. Chen, L. M. Veca and S.-Y. Xie, "Quantum-Sized Carbon Dots for Bright and Colorful Photoluminescence," *Journal of the American Chemical Society*, vol. 128, no. 24, pp. 7756-7757, 2006.

34. L. Yang, Z. R. Wang, J. Wang, W. H. Jiang, X. W. Jiang, Z. S. Bai, Y. P. He, J. Q. Jiang, D. K. Wang and L. Yang, "Doxorubicin conjugated functionalizable carbon dots for nucleus targeted delivery and enhanced therapeutic efficacy," *Nanoscale*, vol. 8, no. 12, pp. 6801-6809, 2016.

35. M. Algarra, B. B. Campos, K. Radotic, D. Mutavdzic, T. Bandosz, J. Jimenez-Jimenez, E. Rodriguez-Castellon and J. C. G. E. da Silva, "Luminescent carbon nanoparticles: effects of chemical functionalization, and evaluation of Ag+ sensing properties," *Journal of Materials Chemistry A*, vol. 2, no. 22, pp. 8342-8351, 2014.

36. T. N. J. I. Edison, R. Atchudan, M. G. Sethuraman, J. J. Shim and Y. R. Lee, "Microwave assisted green synthesis of fluorescent N-doped carbon dots: Cytotoxicity and bio-imaging applications," *Journal of Photochemistry and Photobiology B-Biology*, vol. 161, pp. 154-161, 2016.

37. P. Yu, X. M. Wen, Y. R. Toh and J. Tang, "Temperature-Dependent Fluorescence in Carbon Dots," *Journal of Physical Chemistry C*, vol. 116, no. 48, pp. 25552-25557, 2012.

38. Y. Yuan, B. Guo, L. Hao, N. Liu, Y. Lin, W. Guo, X. Li and B. Gu, "Doxorubicin-loaded environmentally friendly carbon dots as a novel drug delivery system for nucleus targeted cancer therapy," *Colloids & Surfaces B Biointerfaces*, pp. 349, 2017.

Figures

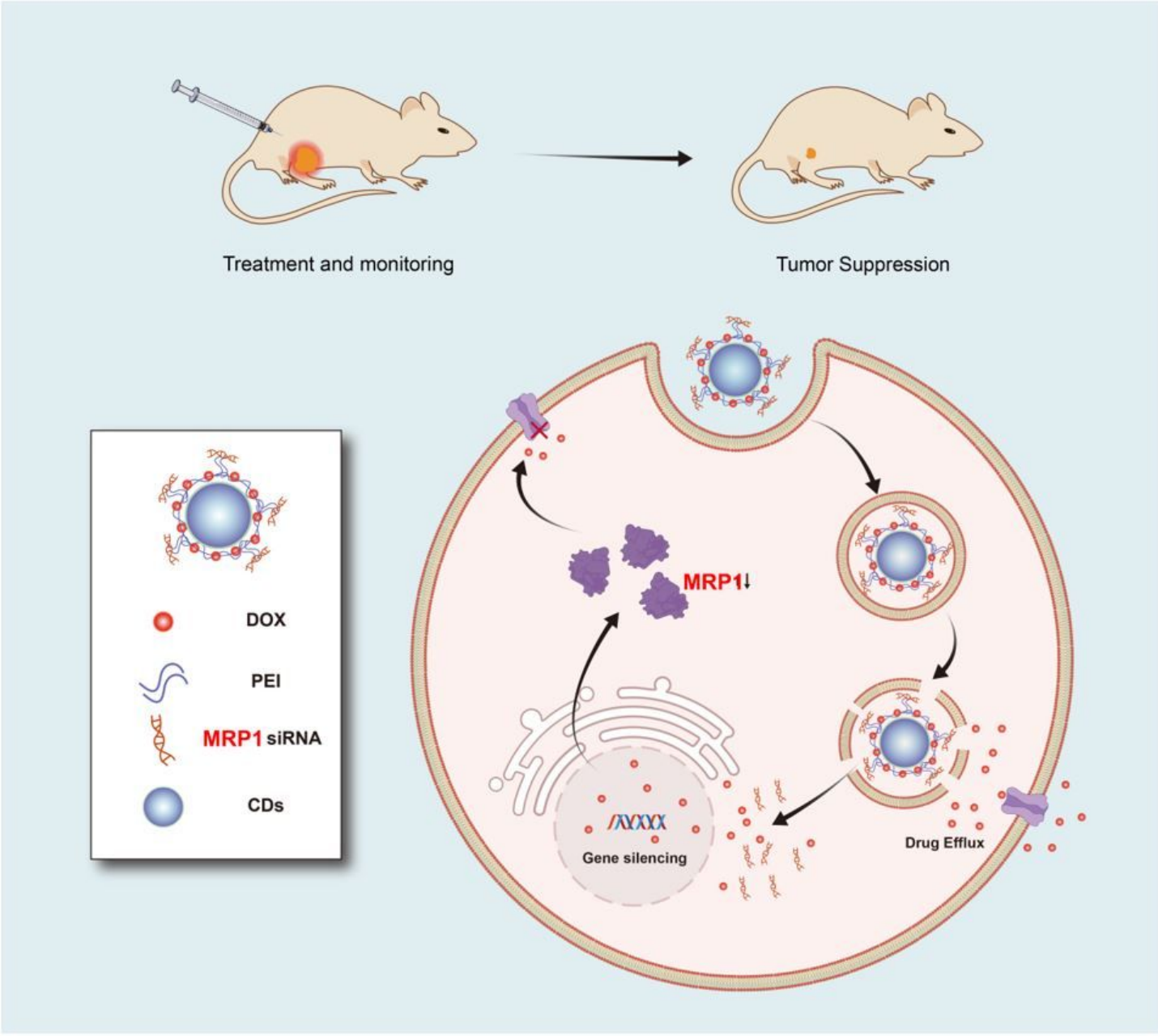

Figure 1

The schematic diagram of CD-PEI-DOX-siMRP1 overcomes the chemoresistance.

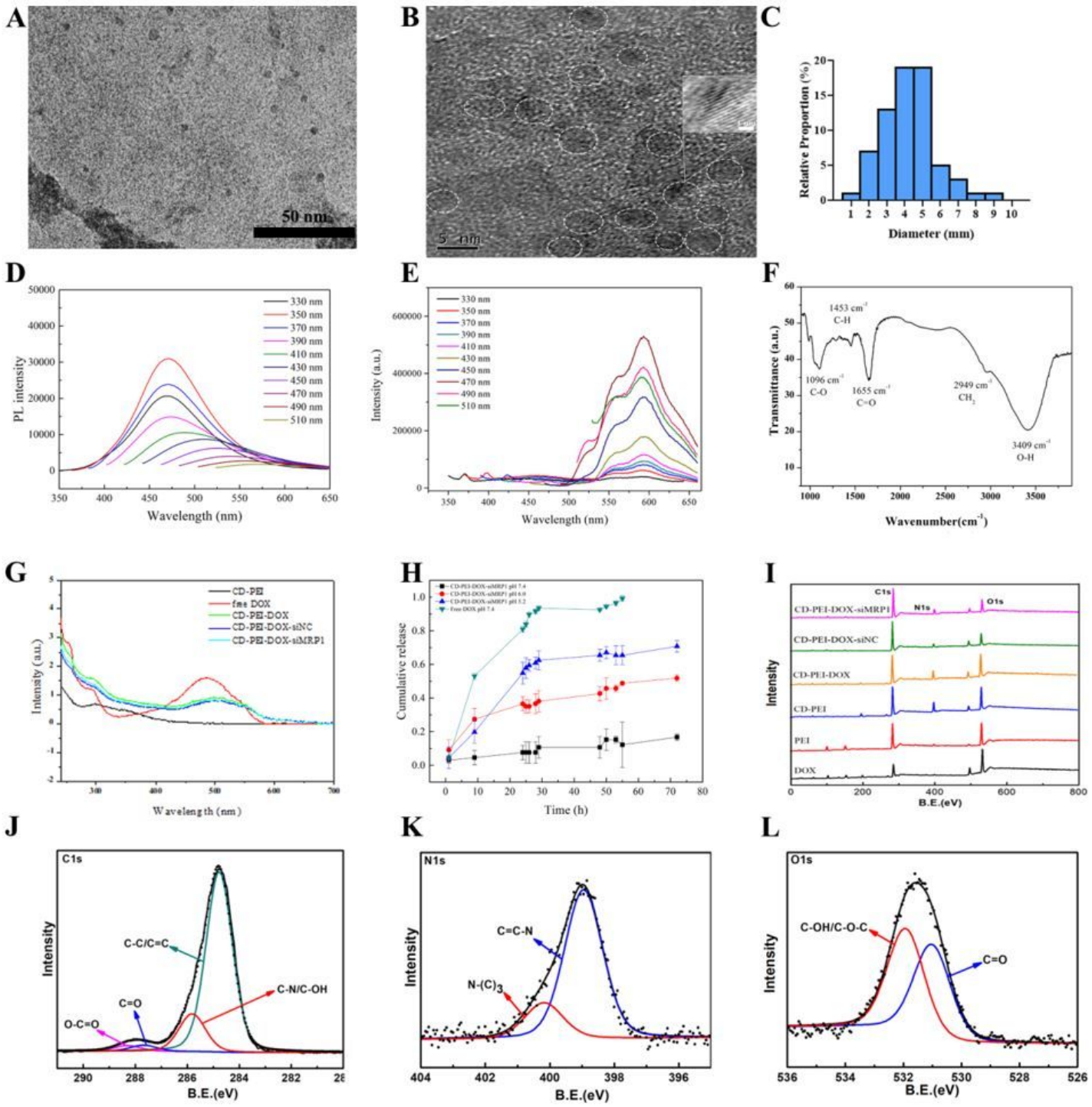

Figure 2

The characteristics of CD-PEI and CD-PEI-DOX-siMRP1. (A) and (B) The TEM images of CD-PEI (the inset is an auto correlation of the TEM image of the marked area using Digital Micrograph software). (C) The diameters distribution of CD-PEI. (D) The PL spectrum of CD-PEI. (E) The PL spectrum of CD-PEI-DOX-

siMRP1. (F) The FTIR spectrum of CD-PEI. (G) The UV-vis spectrum of CD-PEI, CD-PEI-DOX, CD-PEI-DOX-siNC, and CD-PEI-DOX-siMRP1. (H) The release behavior of CD-PEI-DOX-siMRP1 and free DOX under different pH. (I) XPS spectrum of PEI, DOX, CD-PEI, CD-PEI-DOX, CD-PEI-DOX-siNC, and CD-PEI-DOX-siMRP1. (J) C1s, (K) N1s and (L) O1s spectra of CD-PEI-DOX-siMRP1.

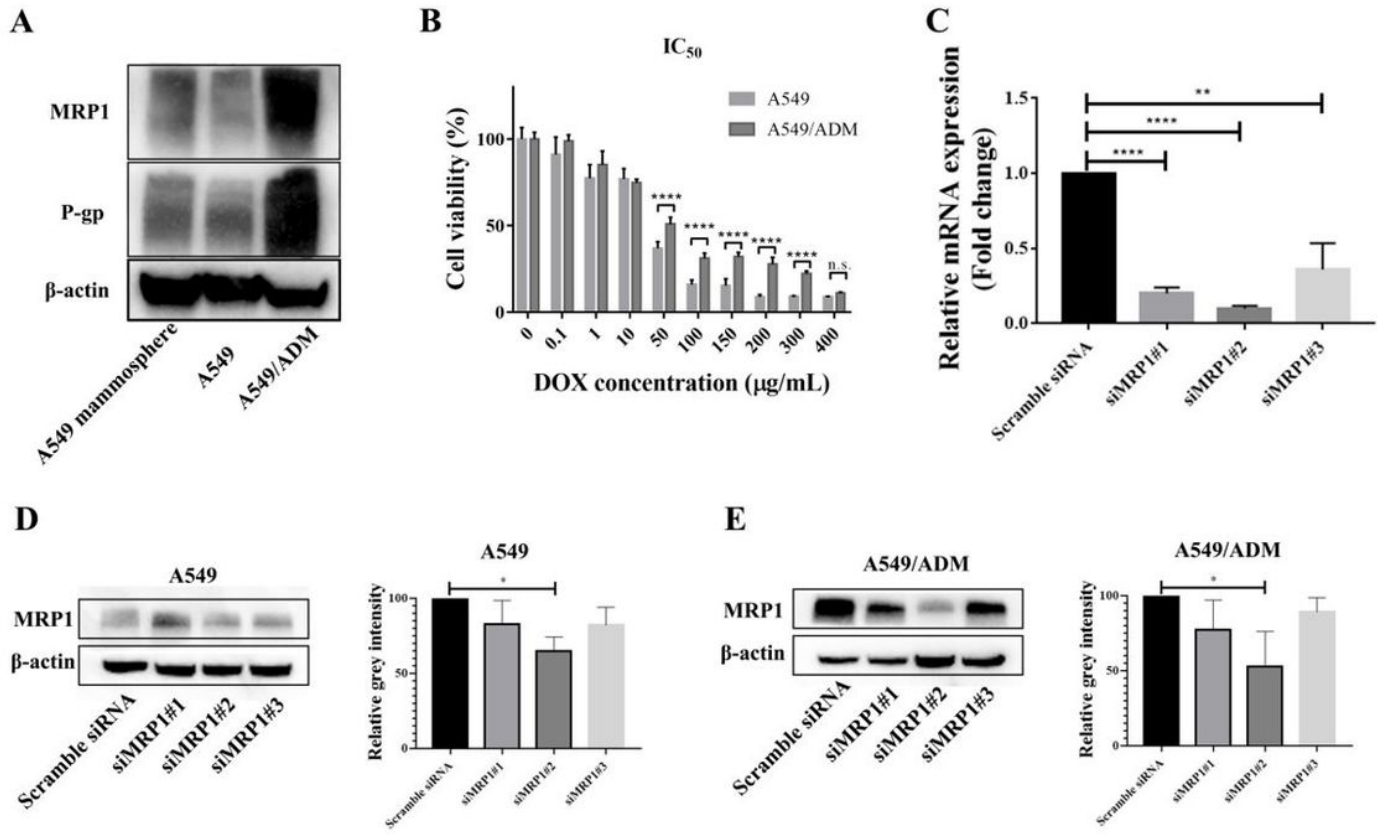

Figure 3

Analysis of chemoresistance of lung cancer cells against doxorubicin. (A) Expression of MRP1 and P-gp on A549, A549 mammosphere, and chemoresistant A549/ADM cells by western blot. β-actin was used as a loading control. (B) Cell viability was detected after treatment by indicated concentrations of doxorubicin in A549 and A549/ADM cells. **** indicates $p<0.0001$. (C) The expression of MRP1 was detected by qPCR after knockdown by three siRNA sequences in A549/ADM cells. (D) The expression of MRP1 in A549 cells was detected by western blot after knockdown by three siRNA sequences. (E) The expression of MRP1 in A549/ADM cells was detected by western blot after knockdown by three siRNA sequences. Quantification of grey intensity from each group was shown.

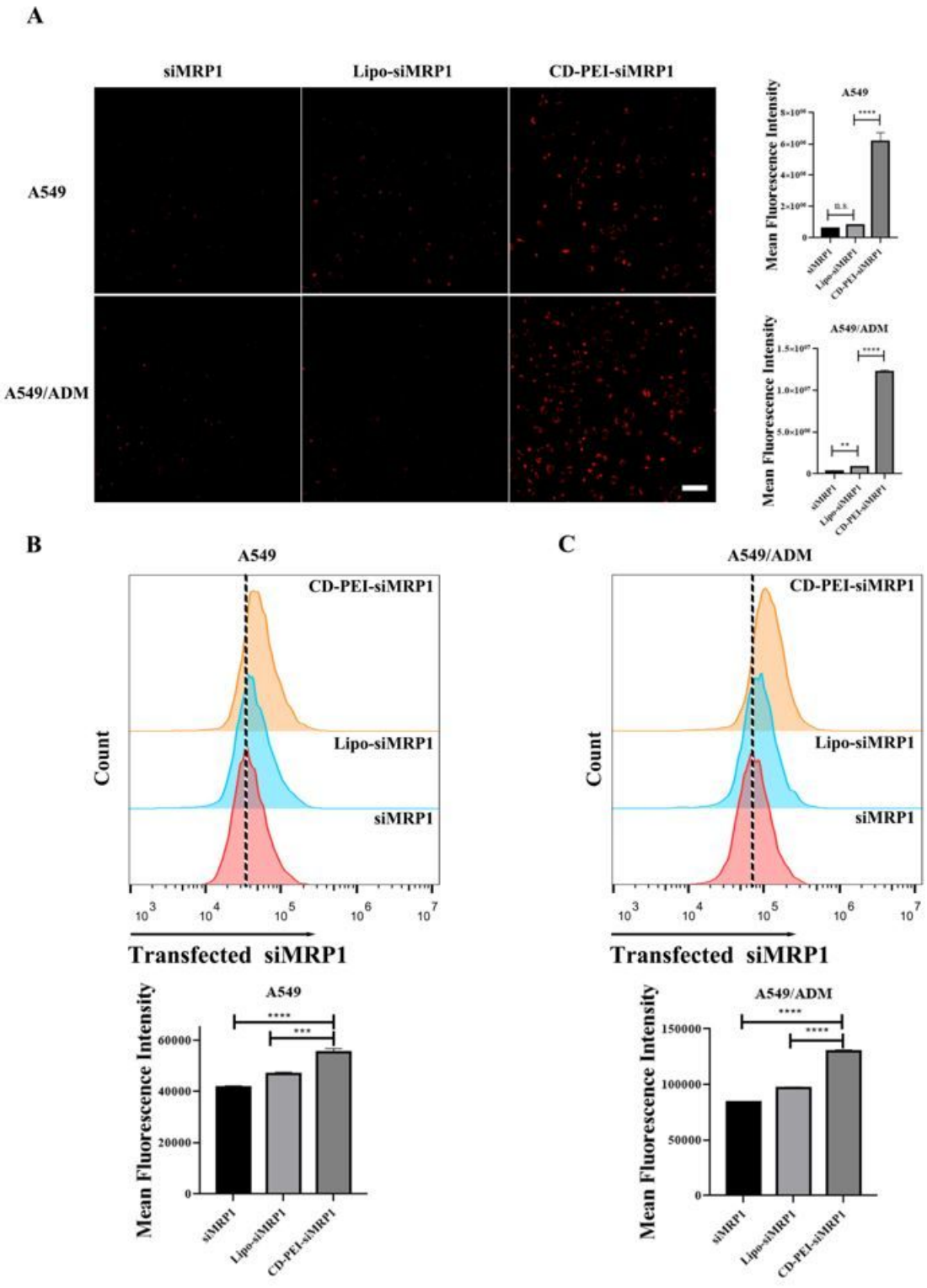

Figure 4

CD-PEI delivered siMRP1 to lung cancer cells efficiently. (A) The transfection efficiency of siMRP1 by lipo or CD-PEI detected by laser scanning confocal microscope. (B) The transfection efficiency and quantification of siMRP1 on A549 cells by flow cytometry. (C) The transfection efficiency and quantification of siMRP1 on A549/ADM cells by flow cytometry. (Scale bar:100 μm)

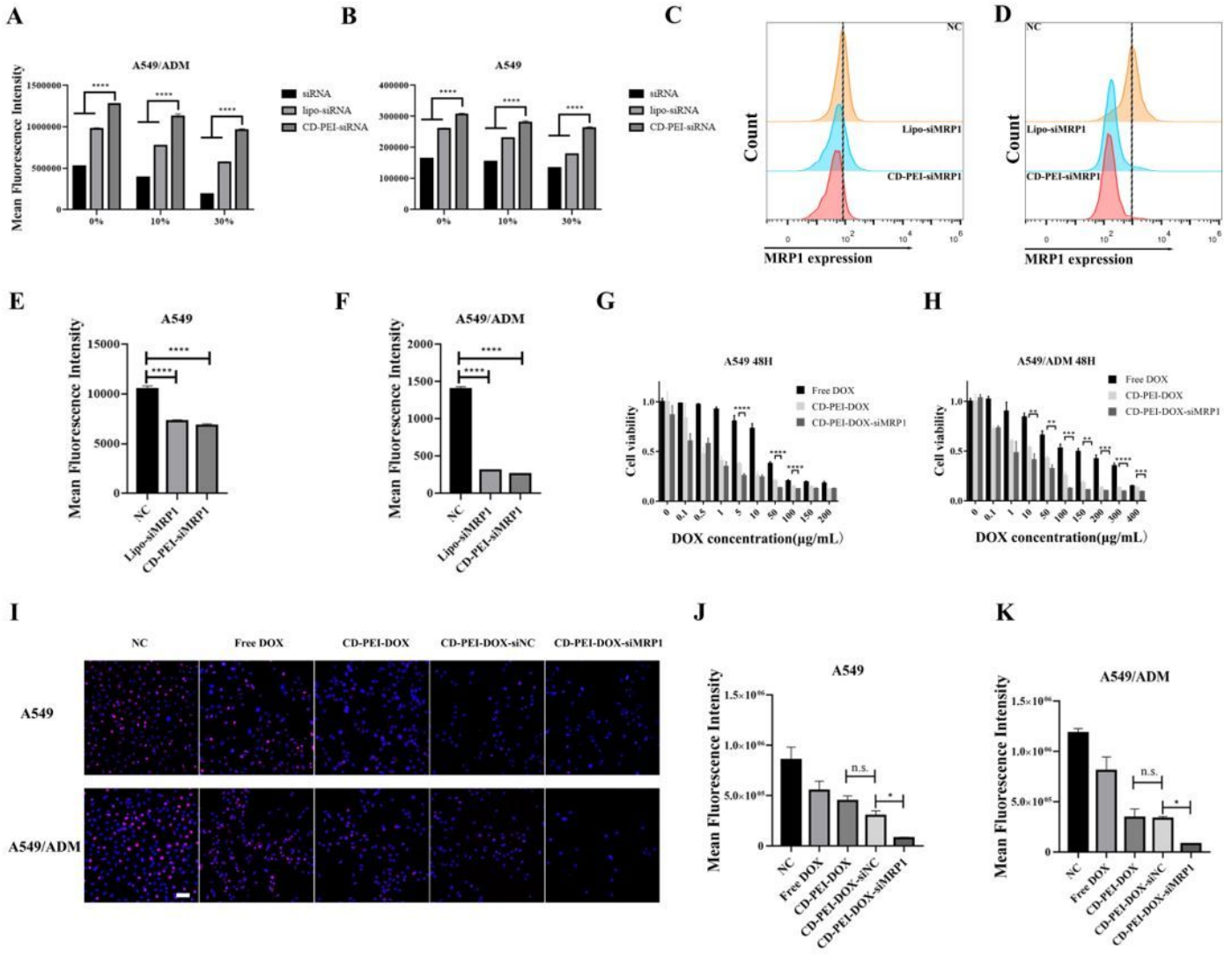

Figure 5

CD-PEI-DOX-siMRP1 inhibits the expression of MRP1 and causes inhibition of proliferation in lung cancer cells. (A) and (B): Detection of transfection efficiency of CD-PEI-DOX-siMRP, Lipo and free siRNA under indicated concentrations of serum. Expression (C) and quantification (E) of MRP1 on A549 cells by flow cytometry. Expression (D) and quantification (F) of MRP1 on A549/ADM cells by flow cytometry. (G-H). The cell viability of A549 and A549/ADM cells incubation with free DOX, CD-PEI-DOX, and CD-PEI-DOX-siMRP1. (I-K) Expression and quantification of Ki67 on A549 and A549/ADM cells by CLSM (Scale bar:100 μm).

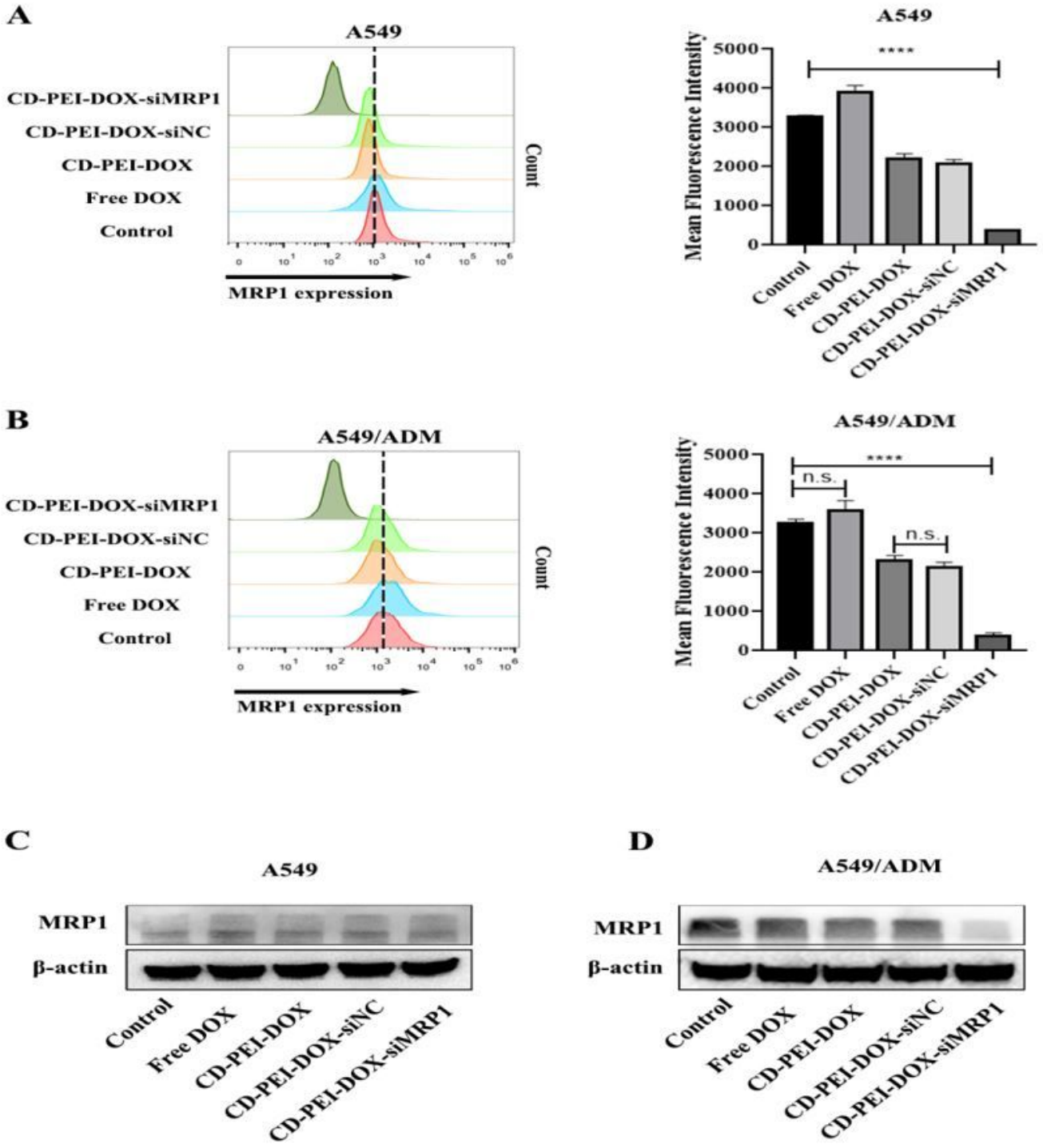

Figure 6

Expression of MRP1 on lung cancer cells treated by different drugs. (A) Expression and quantification of MRP1 on A549 cells by flow cytometry. (B) Expression and quantification of MRP1 on A549/ADM cells by flow cytometry. (C) The expression of MRP1 in A549 cells was detected by western blot. (D) The expression of MRP1 in A549/ADM cells was detected by western blot.

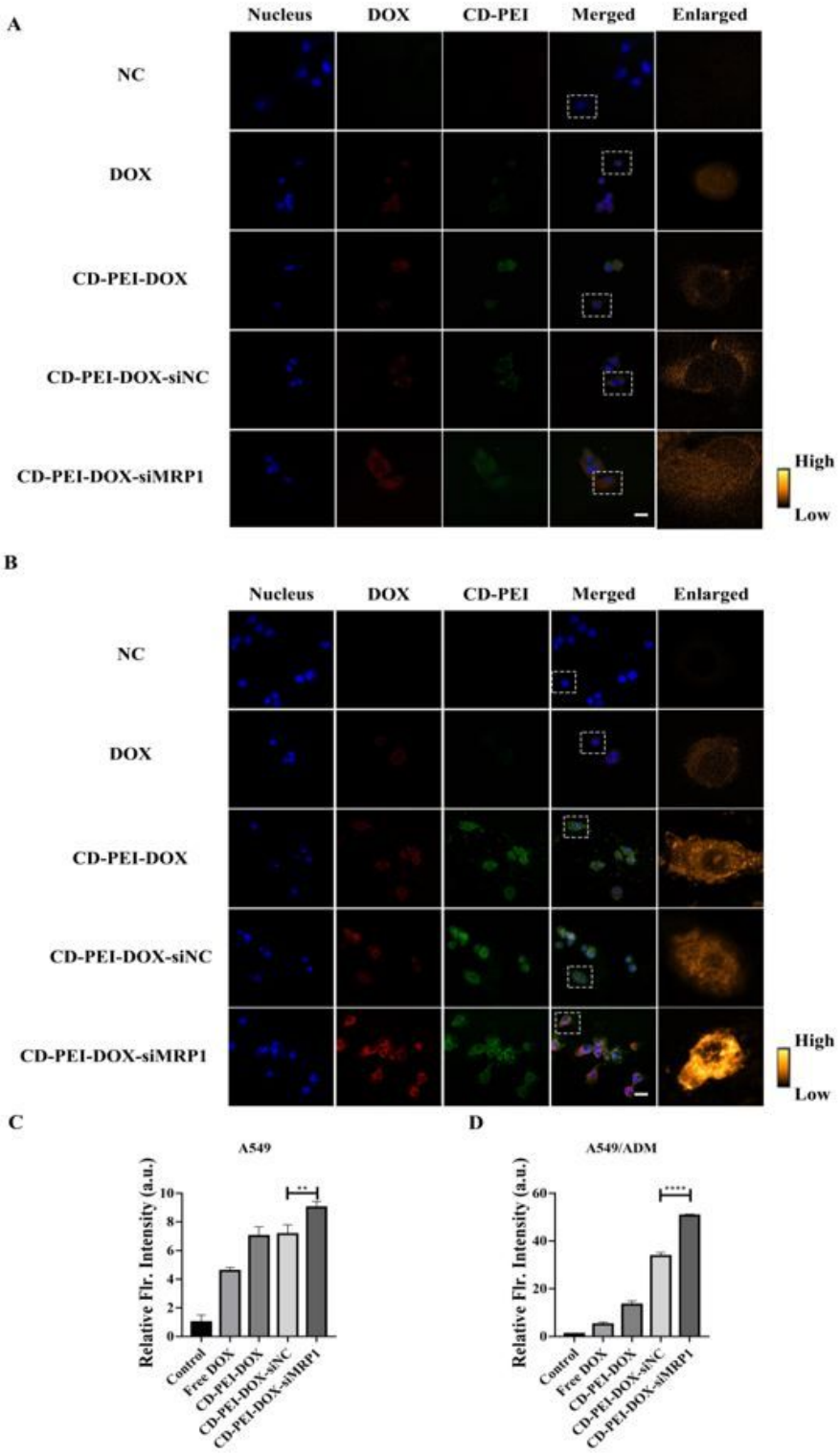

Figure 7

The uptake of cells treated with indicated drugs detected by laser confocal scanning microscopy. A549 (A) and A549/ADM (B) cells were treated with PBS, DOX, CD-PEI-DOX, CD-PEI-DOX-siNC, and CD-PEI-DOX-siMRP1 respectively. Representative pictures were taken under confocal microscopes using 40X oil lens. Blue and red signals indicate nucleus and doxorubicin. CD-PEI was manifested by green signals. Signals were merged using the same field. DOX distribution was reflected by densometric scale as shown in the

fifth panel (Enlarged). (C) and (D) The quantitative analysis of the fluorescence intensity of DOX by ImageJ. The scale bar is 20μm.

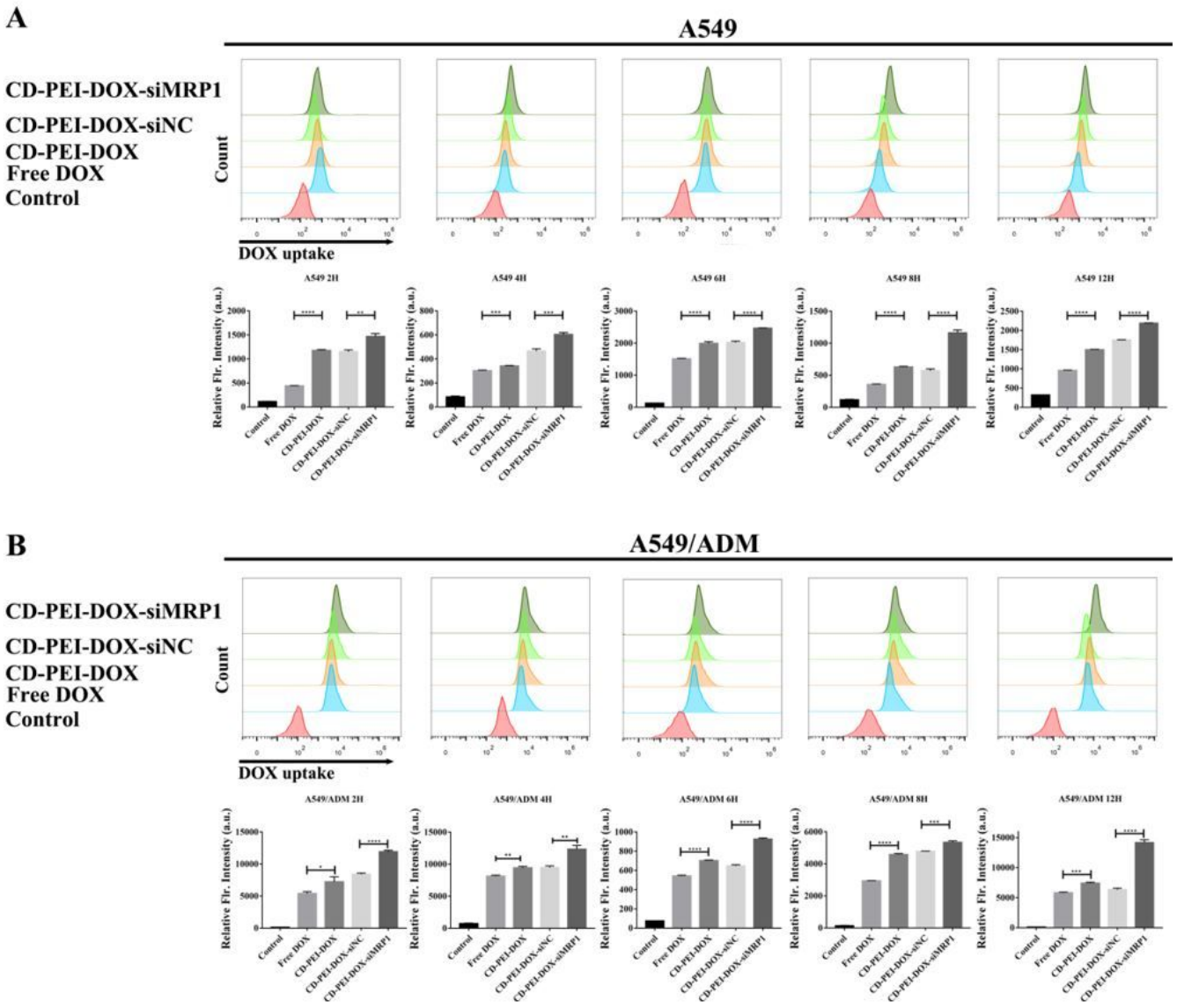

Figure 8

Uptake of drugs in A549/ADM and A549 cells were determined using flow cytometry. (A) Upper panel: A549 cells were treated with the drugs for the indicated periods, cells were collected and fluorescence signal of DOX were detected. Lower panel: Mean fluorescence intensity of each cell were calculated and statistically analyzed. (B) Upper panel: A549/ADM cells were treated with the drugs for the indicated time points, followed by FACs (fluorescence-activated cell sorting) analysis detecting the fluorescence of DOX. Lower panel: Statistically analysis of mean fluorescence intensity of DOX in each group. **** indicates $p<0.0001$.

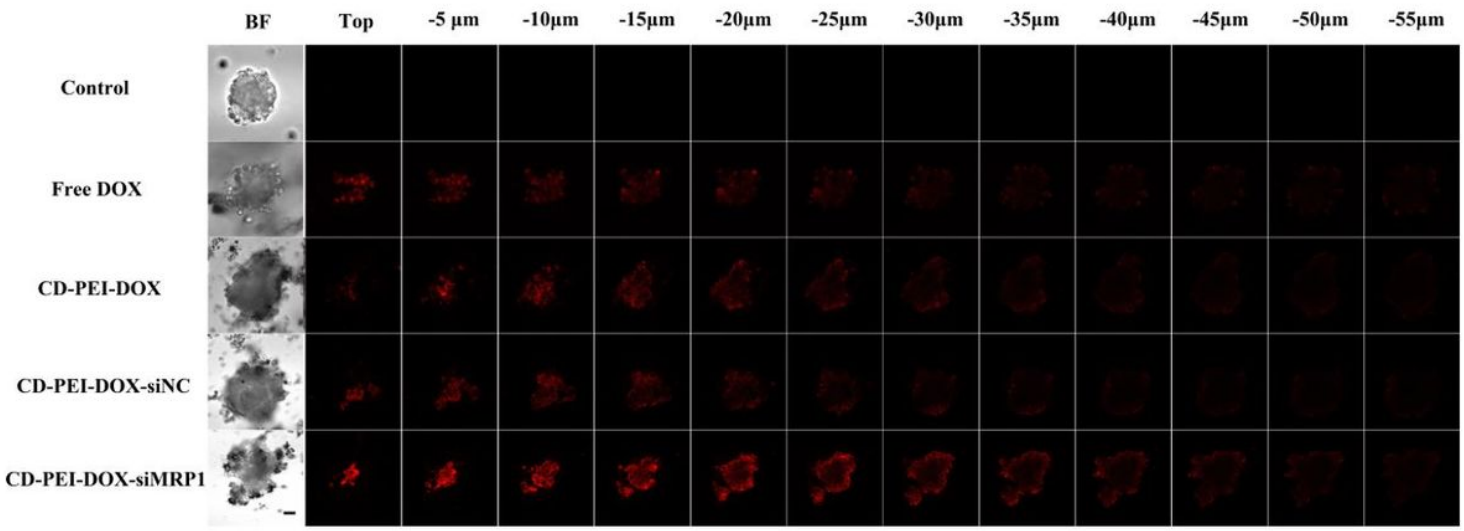

Figure 9

The penetration of drugs was detected using A549/ADM cells. Confocal Z-stack images of cell mammospheres were obtained and shown after incubation with PBS, free DOX, CD-PEI-DOX, CD-PEI-DOX-siNC, and CD-PEI-DOX-siMRP1. The bar is 20 μm.

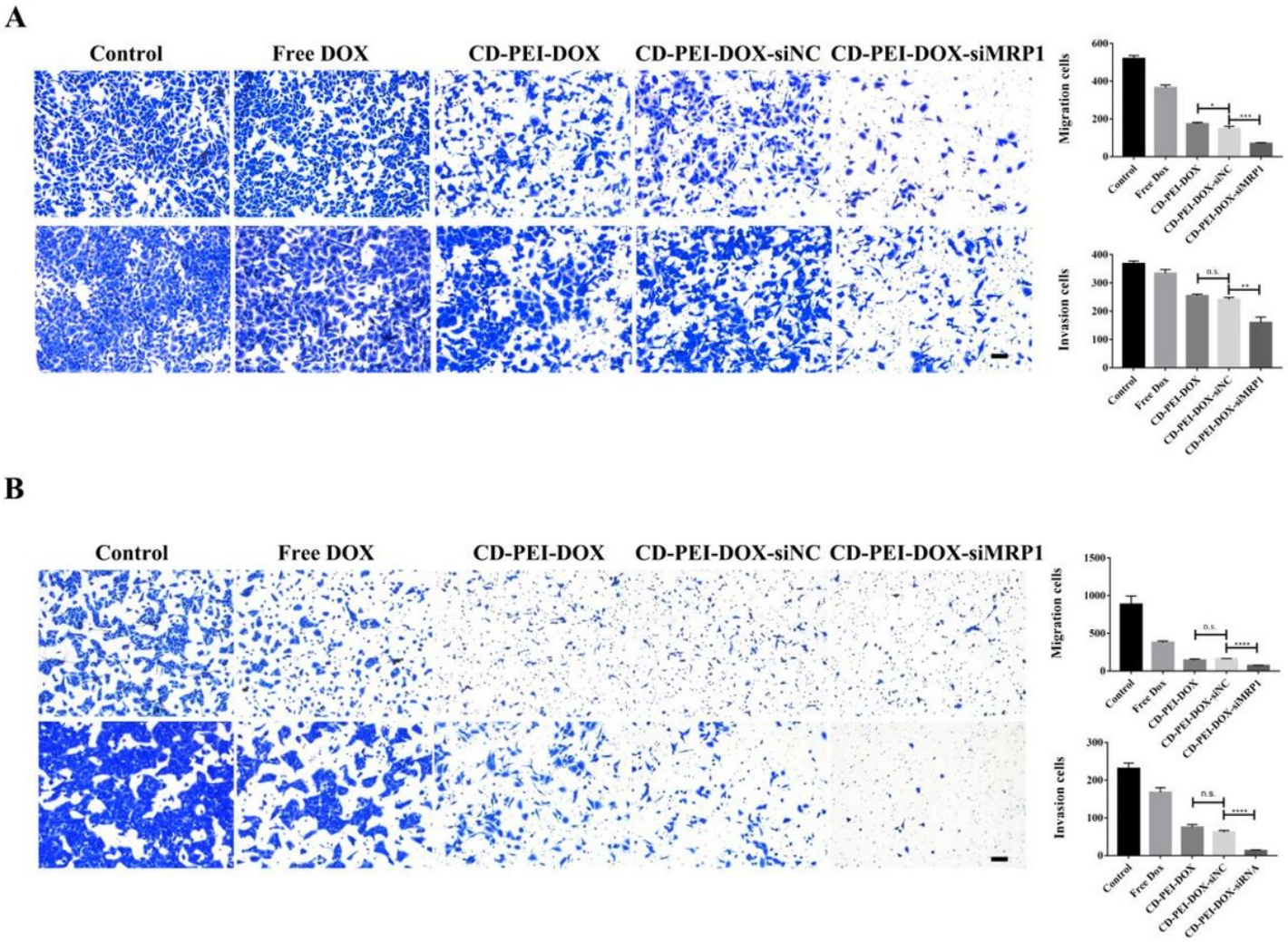

Figure 10

The transwell assay was performed to determine whether CD-PEI or CD-PEI-DOX-siMRP1 enhanced the inhibition effect of DOX. Microscopy images of the migration (Upper) and invasion (Lower) of A549 (A) and A549/ADM (B) cells that passed through the membrane after incubating with PBS, DOX, CD-PEI-DOX, CD-PEI-DOX-siNC and CD-PEI-DOX-siMRP1 compared with the control group (untreated cells). Statistical analyses were shown in the right panel of each figure. * $p < 0.05$. ** $p < 0.01$. *** $p < 0.001$. The scar bar is 200 μm.

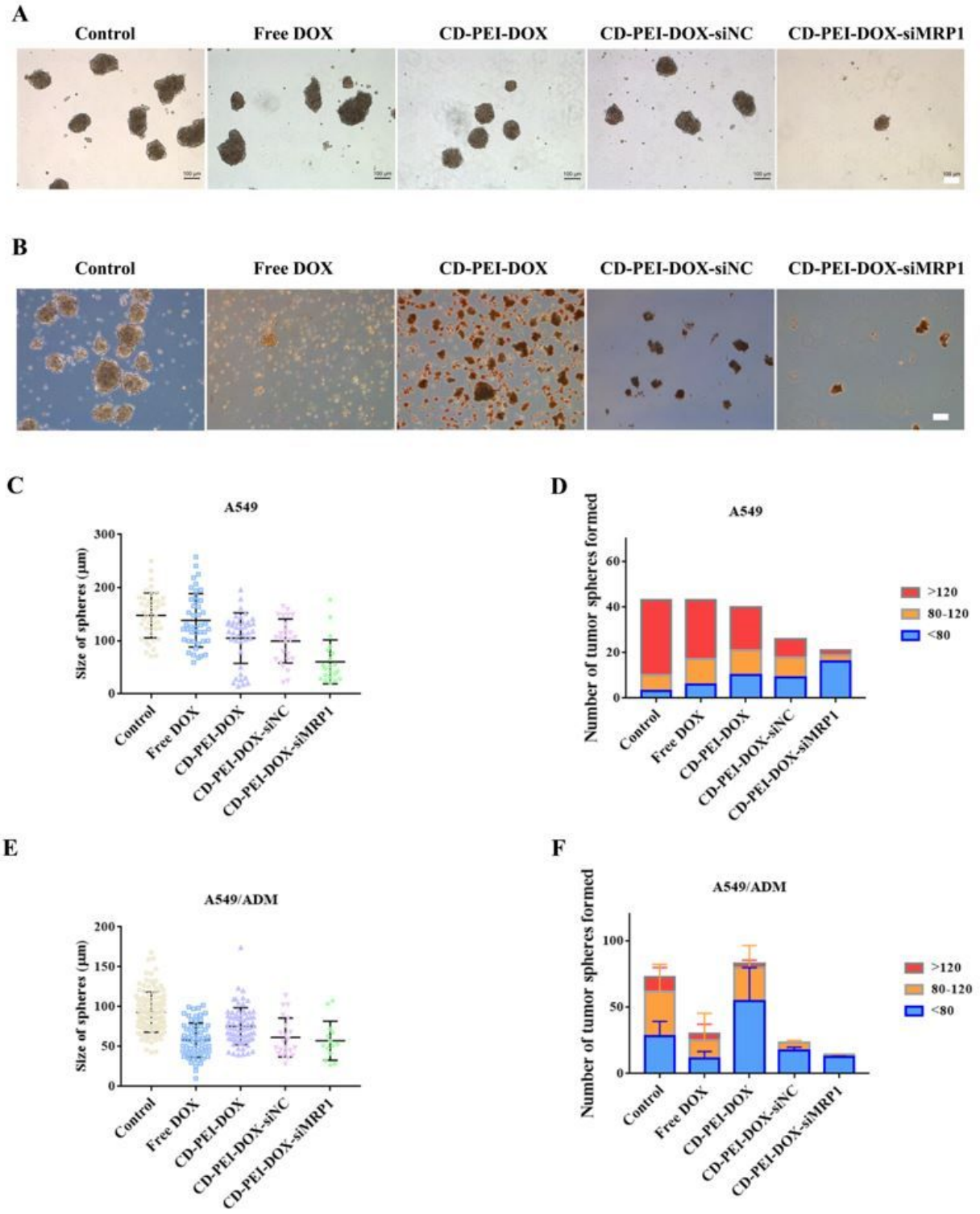

Figure 11

The sphere forming assays of A549(A) and A549/ADM(B) cells treated by PBS, DOX, CD-PEI-DOX, CD-PEI-DOX-siNC, and CD-PEI-DOX-siMRP1. (C) and (D) Relative sizes and numbers of sphere were shown in A549 cells(A). (E) and (F) Relative sizes and numbers of sphere shown in A549/ADM (B). The scar bar is 100 μm.

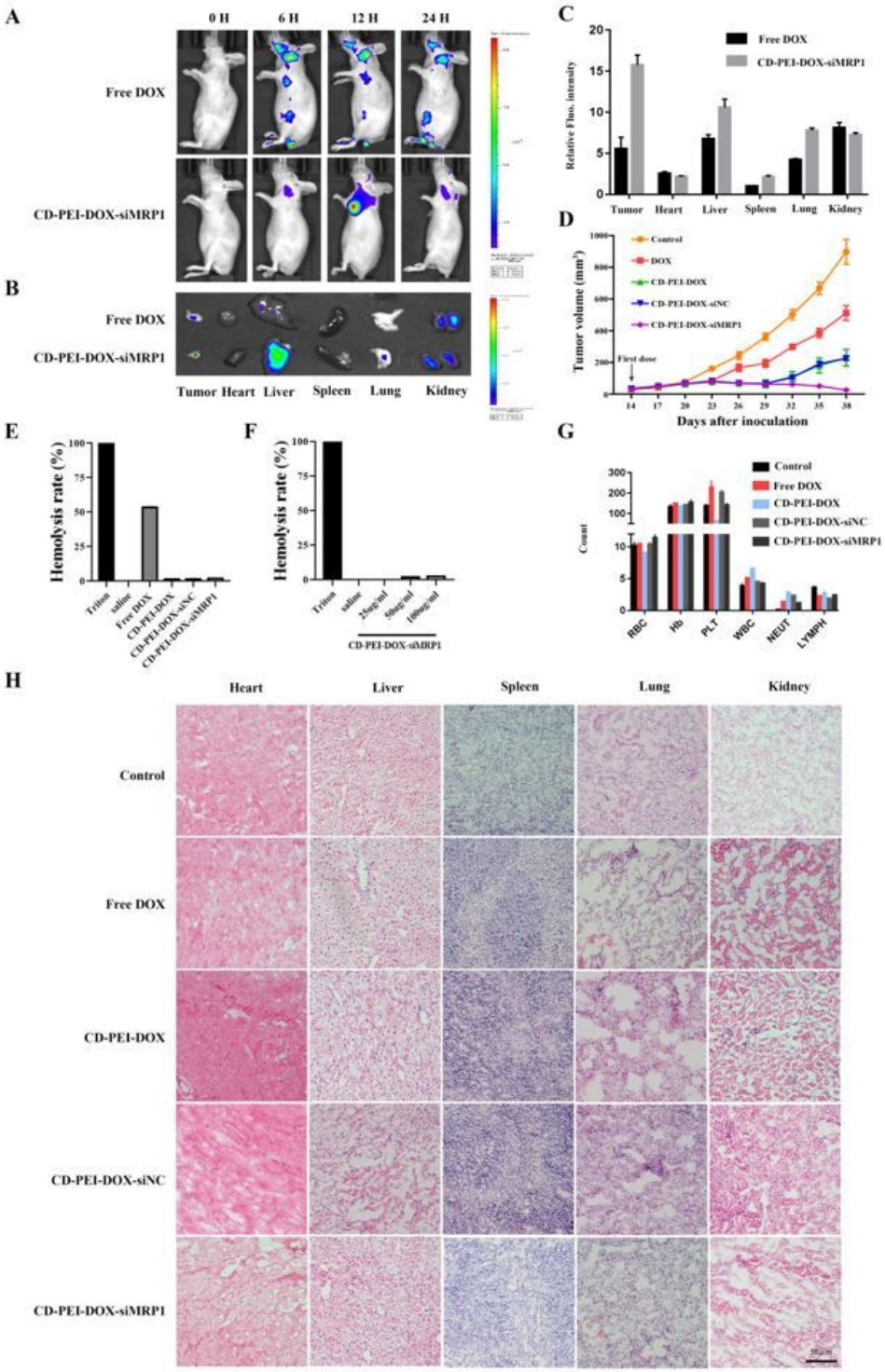

Figure 12

Analysis of targeting and biocompatibility of nanodrugs. (A) Free DOX and CD-PEI-DOX-siMRP1 were injected through tail vein in subcutaneous xenograft model. Pictures of representative time point were taken by IVIS. (B) Tumor and organs of representative group were harvested and photographed under IVIS. (C) Relative fluorescence intensity of each organ were calculated and statistically analyzed. (D) The therapy of CD-PEI-DOX-siMRP1 in vivo. (E) and (F) Hemolysis assays were conducted to analyze the toxic

effect of different drugs as indicated and dose-dependent toxic effect of CD-PEI-DOX-siMRP1 in on blood from volunteer. (G) Blood cells analysis was applied to analyze the biocompatibility of indicated drugs. (H) H&E staining was conducted to determine the toxic effect of various drugs in indicated groups.

Supplementary Files

This is a list of supplementary files associated with this preprint. Click to download.

- Graphicalabstract20210818.docx
- Supportingmaterials.docx